Steel and Composite Structures, *Vol. 19*, *No. 2* (*2015*) *441-465*
DOI: http://dx.doi.org/10.12989/scs.2015.19.2.441

Flexural and compression behavior for steel structures strengthened with Carbon Fiber Reinforced Polymers (CFRPs) sheet

Jai-woo Park [1] and Jung-han Yoo [*2]

[1] *Korea Infrastructure Safety Corporation., 315, Goyang-Daero, Ilsan-Gu, Goyang-city, Gyeonggi-Do, 411-758, Republic of Korea*
[2] *School of Architecture, Seoul National University of Science &Technology, 232 Gongreung-ro, Nowon-gu, Seoul, 139-743, Republic of Korea*

(*Received September 11, 2014, Revised February 02, 2015, Accepted February 06, 2015*)

Abstract. This paper presents the experimental results of flexural and compression steel members strengthened with carbon fiber reinforced polymers (CFRP) sheets. In the flexural test, the five specimens were fabricated and the test parameters were the number of CFRP ply and the ratio of partial-length bonded CFRP sheets of specimen. The CFRP sheet strengthened steel beam had failure mode: CFRP sheet rupture at the mid span of steel beams. A maximum increase of 11.3% was achieved depending on the number of CFRP sheet ply and the length of CFRP sheet. In the compression test, the nine specimens were fabricated and the main parameters were: width-thickness ratio (b/t), the number of CFRP ply, and the length of the specimen. From the tests, for short columns it was observed that two sides would typically buckle outward and the other two sides would buckle inward. Also, for long columns, overall buckling was observed. A maximum increase of 57% was achieved in axial-load capacity when 3 layers of CFRP were used to wrap HSS columns of b/t = 60 transversely.

Keywords: FRP; CFRP; steel beam; Hollow Steel Section (HSS); long column; short column; retrofit

1. Introduction

Fiber reinforced polymer (FRP) materials have been widely used for the repair and strengthening of strengthened concrete structures (Swamy *et al*. 1989, Ritchie *et al*. 1991). Due to the success of strengthened concrete structures, a number of researchers have investigated the use of carbon fiber reinforced polymer (CFRP) materials for repair and strengthening of steel structures and steel-concrete composite structures. Generally, for the repair and strengthening method on the steel structures, steel plate strengthening method has mainly used by bolting and welding between mother material and reinforcement material. In the case of using bolted joint, cross-sectional loss of the base material is caused due to the bolt hole; and, upon performing welded joint; there are many weaknesses such as deformation on the base material due to the

∗Corresponding author, Assistant Professor, E-mail: happyjh@seoultech.ac.kr
[a] Chief of Research Division, E-mail: anm21c@hanmail.net

http://www.techno-press.org/?journal=scs&subpage=8 ISSN: 1229-9367 (Print), 1598-6233 (Online)

welding heat. Also, the steel plate itself is a heavy material, which causes: (1) increase in the self-weight of the structure; (2) reduction of constructability; and (3) vulnerability to corrosion. To solve these weaknesses of the steel plate strengthening method, a study using the FRP (Fiber reinforced polymer sheet) of the steel structure on the repair and strengthening has recently performed, and the repair and strengthening method using this has applied to the field (Park *et al*. 2013). FRP is: (1) light-weight material compared to the steel plate; (2) easy to construct; and (3) has strong corrosion resistance. Also, FRP is (4) high-strength material; therefore a high reinforcement effect is expected with low reinforcement quantity. Moreover, welding or bolt construction is unnecessary, and only the reinforcement using epoxy is required, which has the advantage of construction without base material deformation and cross-sectional loss (Zhao and Zhang 2007).

Considering the study on the FRP repair and strengthening of the steel structure, Miller *et al*. (2001) performed the study of reinforcing the bottom flange of steel beams CFRP (Carbon Fiber reinforced polymer sheet) and GFRP (Glass Fiber reinforced polymer sheet) to increase the flexure performance. Artificial damage of steel sections has been attempted to simulate fatigue cracks (Photiou *et al*. 2006, Shatt and Fam 2008). Fatigue cracks are simulated by introducing a partial or complete saw cut at the bottom flange of steel beams. Some researchers (Schnerch and Rizkalla 2008, Fam *et al*. 2009, Harries *et al*. 2009, Sallam *et al*. 2010) investigated the FRP strengthening effect for the steel-concrete composite beams. Schnerch and Rizkalla (2008) performed the study of applying high modulus CFRP strips to reinforce the lower flange of the composite beam to verify the flexural reinforcement effect. Sallam *et al*. (2010) strengthened the CFRP sheet on the bottom flange of the composite beam to perform the flexural behavior test. Here, to increase the bonding performance of the CFRP sheet and the steel surface, the CFRP sheet was wrapped for reinforcement to perform the flexural performance test. As a result of considering the preceding studies, most are applying FRP reinforcement on the steel-frame flexural member, and most are focusing on FRP reinforcement on the bottom flange to verify the flexural performance. In this study, flexural performance evaluation was performed in the case of using CFRP on the steel beam for the partial-length reinforcement. Through this, the steel beam with partial-length reinforcement was observed of the strengthening effect and the failure mode through the flexural test. Also, as a result of previewing the preceding studies, most studies on the steel frame-FRP reinforcement have focused on the flexural member, and studies on the FRP strengthening effect of the compression member were not observed. A study on the CFRP reinforcement of partial steel-frame compression member was performed by Shatt and Fam (2006, 2009), but there are no studies on the steel-frame compression member for slender section with high width to thickness ratio. Therefore, in this study, axially loaded compression test was performed to verify the strengthening effect through the CFRP reinforcement on the compression member composed of HSS (Hollow square section). In the AISC provisions (AISC 2010), the compression member is classified into non-compact section and slender section for each width to thickness ratio according to the load condition and the cross-section shape. The non-compact section has local buckling after the yield strength of the steel to result in failure, but the slender section has local buckling before the yield strength of the steel to result in failure. Therefore, in this study, to compare and verify the FRP reinforcement effect of the non-compact section and the slender section of the compression member, two-types of width to thickness ratio (23, 60) were adopted to perform the centrally compression test. First, for the short-column, b/t = 23 cross-section, which is less than the limitation of width-thickness ratio ($b/t = 1.40\sqrt{E/F_y}$) of the non-compact section of hollow square section (HSS) subjecting to uniform compression, and the HSS over the limitation of width-thickness ratio having b/t = 60 slender section, were selected. Also, to observe the effect according to the slenderness ratio related to the length of the compression member, for the non-compact section HSS, a short-column and long column specimens were produced and strengthened with CFRP sheet to verify the strengthening effect on the long-column.

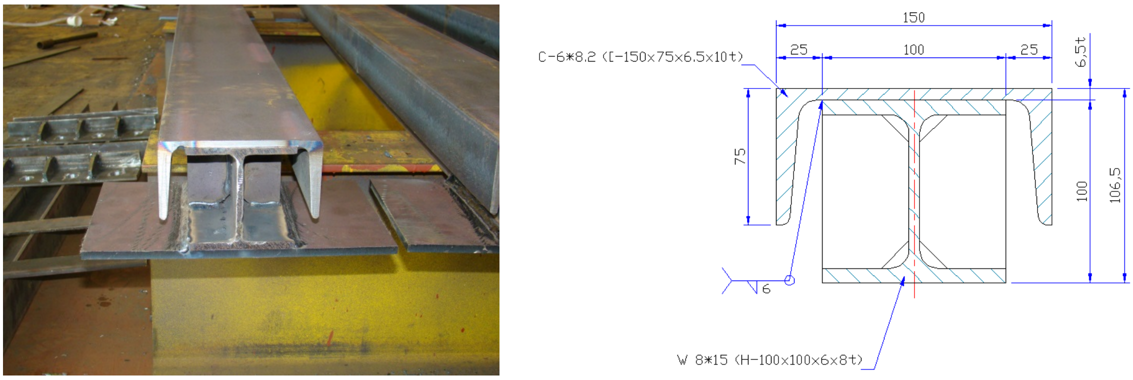

(a) Specimen cross-section and detail

(b) Sand blasting

(c) CFRP sheet application

(d) Specimen fabrication

Fig. 1 Specimen fabrication procedure

Table 1 Parameter plan and flexural test result summary

Specimen label	*W* index Eq. (1)	CFRP retrofitting length		Yield strength (kN)	Gain in yield strength (%)	Failure strength (kN)	Gain in failure strength (%)	Stiffness (kN/mm)	Gain in stiffness (%)
		1ply	2ply						
B0	0	-	-	82.0	-	-	-	8.20	-
B1	0.264	1.0 L	-	100.0	21.9	106.5	-	8.33	1.59
B2	0.528	1.0 L	1.0 L	110.0	31.7	120.5	11.30	8.46	3.17
B2-50%	0.528	1.0 L	0.5L	97.0	18.2 (-11.8)	108.0	1.41 (-10.4)	8.08	-1.46
B2-75%	0.528	1.0 L	0.75 L	105.0	28.0 (-4.5)	111.0	4.20 (-7.9)	8.75	6.71

* Note:
L = length of span
Yield load increase rate: Standard of B0 specimen
Increase rate in FRP failure: Standard of B1 specimen
The result value in ( ) is the increase rate in comparison to the B2 specimen

2. Flexural test

2.1 Test plan

2.1.1 Test parameters and preparation

For the flexural test, a total of 5 steel beams were fabricated and the cross-section of the steel used was W-8×15 (H-100×100×6×8). The test parameters were the number of CFRP layers and the reinforcement length. The span length of the specimen was 1,800 mm, and to prevent lateral-torsional buckling, C-6×8.2 (C-125×65×6×8) was welded to the upper *W* section to be attached, as shown in Fig. 1(a). There was one control specimen (B-0), and other specimens were strengthened with CFRP sheet on the 1-layer and 2-layer (B-1, B-2) on bottom of flange, as shown in the test parameter plan in Table 1. Before the CFRP sheet reinforcement, the rust on the steel surface was removed with the sand bluster, as shown in Fig. 1 (b); afterwards, on the bottom flange, the CFRP sheet was attached using the epoxy, as shown in Fig. 1(c). Also, to observe the flexural performance according to the reinforcement length, on two specimens, first the 1-layer of the CFRP sheet was completely attached, and upon performing the second reinforcement, only the 50% and 75% (800 mm, 1350 mm) of the span length were strengthened to produce the specimens (B2-50%, B2-75%). Moreover, for the shear reinforcement of the loading point and the support, the stiffener was welded to the *W*-section web at the support point of beams. The force equivalence index (ω) was introduced to quantity of the amount of CFRP reinforcement on the basis of CFRP rupture and a relative strength of the CFRP and steel flanges, and the force equivalence index (ω) are expressed in Eq. (1).

$$\omega = \sum_{i=1}^{n} \frac{A_{fi} F_{fi}}{A_{sf} F_y} \tag{1}$$

Where, A_{fi} and F_{fi} are the strengthening area on the CFRP n-layer number and the tensile strength on CFRP failure, and A_{sf} and F_y are the area of the bottom flange and the yield stress of the bottom flange.

2.1.2 Material test

Tables 2 and 3 summarize the material test results of steel plate and CFRP sheet.

Material test results for *W*-section steel plates showed that the yield strength (F_y) was 317 MPa, tensile strength (F_u) was 454 MPa, and the elongation was 30%.

CFRP material properties provided by manufacturer; the average thickness was 0.184 mm/ply, tensile strength was 2696 MPa, and modulus of elasticity was 224.6 GPa. The value for typical thickness of a lamina (a single layer of fabric, wetted with resin and cured) was 0.5 mm-1.0 mm.

2.1.3 Test setup and instrumentations

In the five specimens, the span length as the simple beam was 1800 mm. The load was given with the 500 kN-level actuator on the mid-span section, and to measure the vertical displacement of the center point, one LVDT (linear variable differential transformer) was installed. To measure the strain, the strain gauge was installed in the plan shown in Fig. 2. First, to measure the change process of the neutral axis, three strain gauges were installed on the central web part of the W-section span in the longitudinal direction at a 30 mm distance. On the bottom flange, a strain gauge was installed. The Actuator loading rate is 5.0 mm/min. Fig. 2 shows the schematic diagram for the measuring instrument. To measure the displacement of the mid-span section of the flexural member according to the loading, one LVDT was installed in the center of the specimen as shown in Fig. 2(a); Fig. 2(b) shows the set-up of the specimen.

2.2 Test results and discussion

2.2.1 Failure behavior and load-displacement curve

All specimens all had flexural failure in the mid-span section; sufficient plastic behavior was performed. For the strengthened specimen (B1, B2, B2-50%, B2-75%), the load value gradually increased in the initial loading and CFRP sheet was ruptured after the elastic region and the load value decreased rapidly (Fig. 3(a)). After the CFRP sheet completely ruptured, CFRP sheet delamination was observed on the steel surface (Figs. 3(b) and (c)). For all strengthened specimens, Fig. 3(d) shows the failure shape of all specimens, and as seen in Fig. 3, after the CFRP sheet

Table 2 Material properties of steel plate

Steel thickness (mm)	Actual steel thickness (mm)	Elastic modulus (GPa)	Yield strength (MPa)	Ultimate strength (MPa)	Elongation percentage (%)
8.0	8.0	210	317	454	30

Table 3 Material properties of CFRP

Tensile strength (MPa)	Elastic modulus (GPa)	Ultimate strain (%)	Thickness per ply (mm)
2696	224.6	1.2	0.184

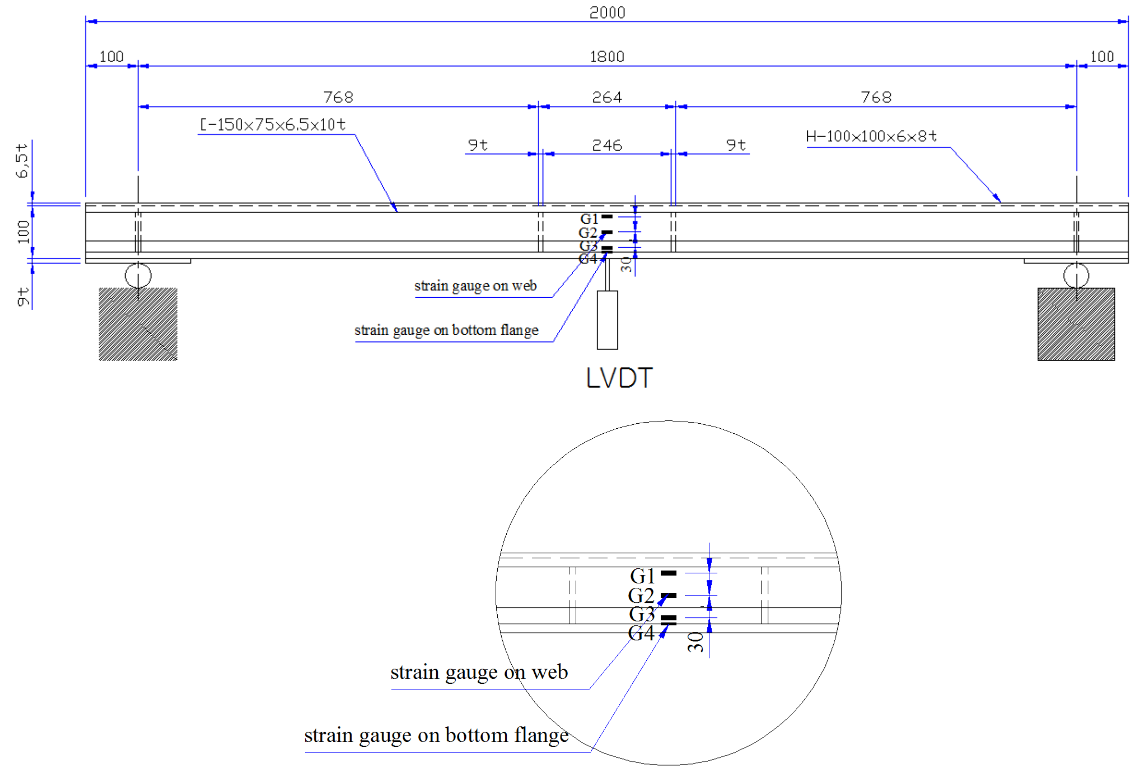

(a) Strain gauge distribution plan

(b) Test setup

Fig. 2 Strain gauge distribution plan and test setup

rupture in the mid-span section, delamination failure had progressed. There was no local buckling in any section of the specimens.

Fig. 4 shows the load-displacement curve on each specimen. Due to the actuator capacity, the maximum strength in the plastic section was not observed, and the maximum displacement was loaded up to 250 mm to observe the behavior.

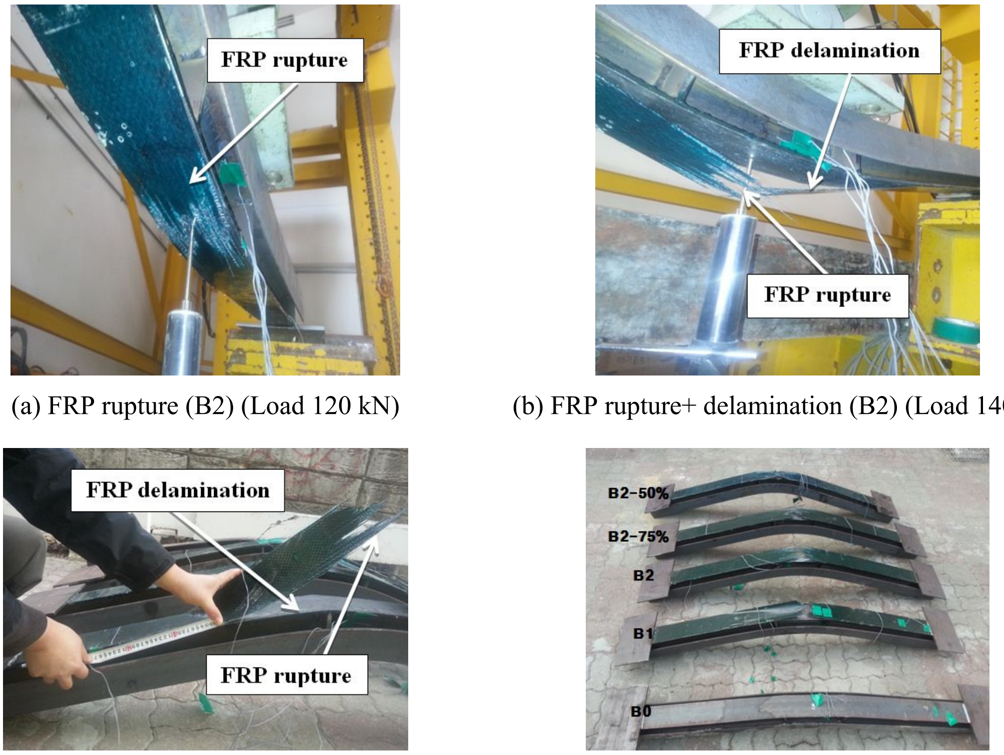

(a) FRP rupture (B2) (Load 120 kN) (b) FRP rupture+ delamination (B2) (Load 140 kN)

(c) FRP rupture + delamination (B2-75%) (d) Final failure shape

Fig. 3 Specimen failure procedure and shapes

In the B-0 specimen, linear behavior was shown in the initial loading section and had non-linear behavior after the yield point, and increase in load was observed according to the increase in displacement. The strengthened specimen also showed linear behavior in the initial loading stage, and was observed to increase in yield load more than the B-0 specimen. After the yield load, non-linear behavior was shown and observed to increase in load, but to decrease rapidly at some point; this the point was the CFRP sheet rupture point. In the B1 specimen, B2 specimen, B2-50%, and B2-75% specimen, the CFRP rupture points were 106.5 kN, 120.5 kN, 111 kN and 108 kN, respectively. After the failure, the load was observed to decrease rapidly, and as the number of CFRP sheet layers increased, the brittle behavior effect of increasing in strength degradation ratio was clearly shown.

2.2.2 Strength and stiffness effect on number of CFRP layer

Table 1 shows the value of yield load and the failure load for each specimen. Here, the failure strength is defined as the load value in the failure point of the CFRP sheet. Also, the yield load (P_y) is defined as shown in Fig. 5. Moreover, the failure load is defined as the load value in the failure point of the CFRP sheet.

The yield load of the B0 specimen calculated by the concept in Fig. 5 was 82 kN, and in the case of B2 specimen, the yield load was 110 kN, showing approximately 31.7% of strength increase effect to verify the flexural reinforcement effect of the CFRP sheet. The reinforcement

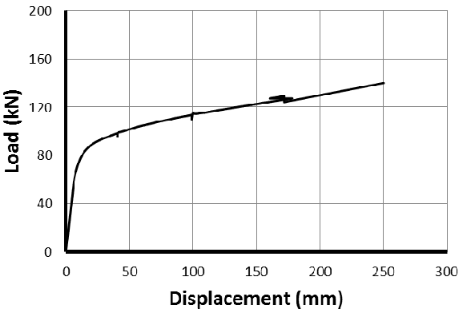

(a) B-0 specimen

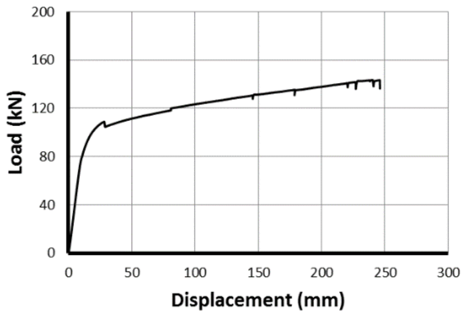

(b) B-1 specimen

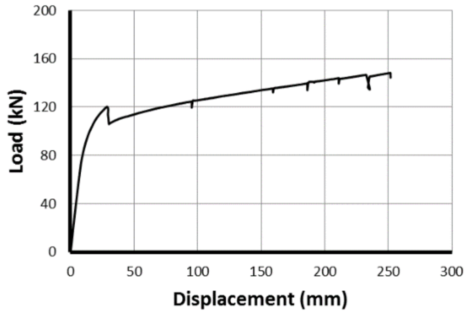

(c) B-2 specimen

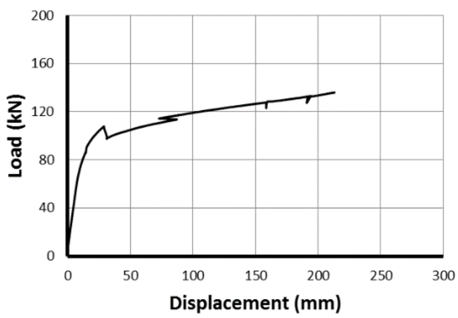

(d) B-2-50% specimen

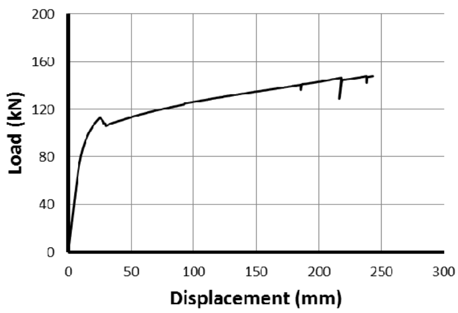

(e) B-2-75% specimen

Fig. 4 Load-displacement curve

effect according to the increase in strength showed the tendency to increase according to the increase in the number of CFRP layer of the CFRP sheet. In the failure point of the CFRP sheet of failure load, the B1 specimen was 106.5 kN; t1

The B2 specimen was 120.5 kN (an increase of approximately 11.3%) to show that the failure load increased according to the increase in the number of CFRP layers. Fig. 6 shows the relation of the force equivalence index (w) calculated in the Eq. (1) contrast to the yield load and failure load of the specimen. As seen in the figure, the load showed an increasing tendency as the reinforcement ratio was increased.

The stiffness value of each specimen was calculated by the concept in Fig. 5, and defined as shown in Eq. (2).

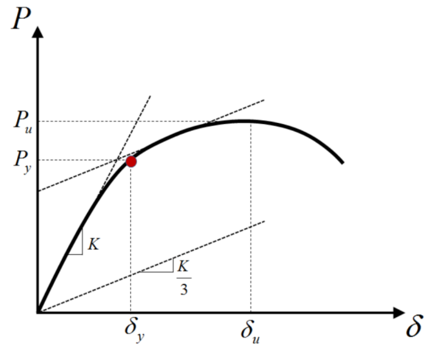

Fig. 5 Definition of yield strength and stiffness

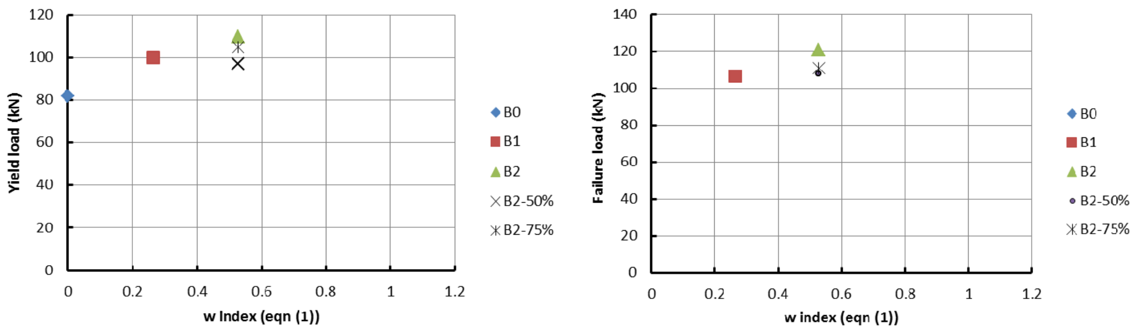

(a) Effect of ω index on yield strength (b) Effect of ω index on failure strength

Fig. 6 Effect of ω index on strength

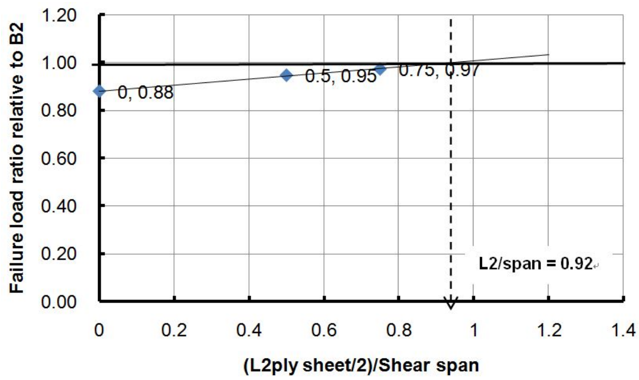

Fig. 7 Effect of strengthening length of CFRP on failure load

$$K_i = \frac{P_y}{\delta_y} \tag{2}$$

The result value found in Eq. (2) is shown in Table 1, as well as the change rate of the stiffness contrast to the B0 specimen. As the analysis result, a maximum of 6.71% and minimum of -1.46% differences were shown contrast to the B0 specimen, and the conclusion of CFRP strengthening not affecting the initial stiffness was derived.

2.2.3 Strength effect on CFRP strengthening length

In strength analysis according to the reinforcement length, the yield load of the B2-50% specimen was 97 kN and failure load was 108.0 kN, a 31.7% and 11.3% increase from each in comparison to the B1 specimen. However, in comparison to the B2 specimen, the yield load decreased 11.8%, and the failure load decreased 10.4%. The B2-75% specimen increased 28.0% in yield load compared to the B0 specimen. However, in comparison to the B-2 specimen with the same number of CFRP layers, the yield load decreased 4.5%. Also, the failure load showed to increase 4.2% compared to the B-1 specimen, but when comparing with the B-2 specimen, 7.9% decrease was shown to verify that the reinforcement length affects the strength. When we look at the *w* index = 0.528 section in the horizontal axis in Fig. 8, the failure strength are decreased according to the decrease in 2-ply reinforcement length. This is considered to be because of the reinforcement in shorter reinforcement length compared to the B-2 specimen to decrease bond stress between the FRP sheets.

Fig. 7 shows the comparison of the failure load of B2 specimen in contrast to the failure strength of the B1 specimen and B2-75% specimen. Here, the horizontal axis of the graph is the ratio of the reinforcement length of the second CFRP sheet length and the span length, and in the case of B-1 specimen, the reinforcement length of the CFRP sheet can be assumed by converting to 0. The strength ratio of B2-75%, B2-50%, and B1 specimens in contrast to the B2 specimen are shown in dots in the graph and the trend line in the three points of B1, B2-75%, and B2-50% are shown in Fig. 7. The load was decreased due to the decrease in the reinforcement length, and the length of the spot meeting the trend line with the load of the B2 specimen to maintain the original load was the reinforcement length restoring the load. Further, when the reinforcement was done in 92% reinforcement length contrast to the original length, we could see that the strength could be restored.

2.2.4 Strain distribution across mid-span section

Fig. 8 is the neutral-axis trend relation curve per load level obtained from the strain gauge installed on the mid-span section of the B0, BF2, and BF2-75% specimens. The strain gauge position installed on the upper part of the bottom flange was 8mm, and strain gauge was installed in the web at a 30 mm distance each. The neutral-axis trend was arranged for each 30 kN level (measure in 15 kN unit for the B0 specimen), and for the strengthened specimen, the neutral-axis trend of the load level was arranged in CFRP sheet failure.

Fig. 8(a) shows the strain distribution across mid-span section for B0 specimens. It could be seen that the strain variation was almost linear throughout stage from 0 kN to 60 kN. The neutral-axis was shifted was observed to move up at 75 kN stage. Finally, at 90 kN stage, large strain was observed at the bottom flange of the beam.

Fig. 8(b) shows the strain distribution across mid-span section for B2 specimens. It can be seen that the strain variation was almost linear throughout stage from 0 kN to 60 kN. At 90 kN stage, it was seen that the neutral-axis was shifted to move up. However, unlike B0 specimen, large strain was not observed at 90 kN stage. This indicates that the CFRP was strongly bonded and kept bearing the load until the final loading stages without significant slippage. At 120 kN stage, large strain was observed at the bottom flange of the beam and CFRP was ruptured.

Fig. 8(c) shows the strain distribution across mid-span section for B2-75% specimens. It can be seen that the strain variation was almost linear throughout stage from 0 kN to 60 kN. At 90 kN stage, it was seen that the neutral-axis was shifted to move up. Large strain was also not observed

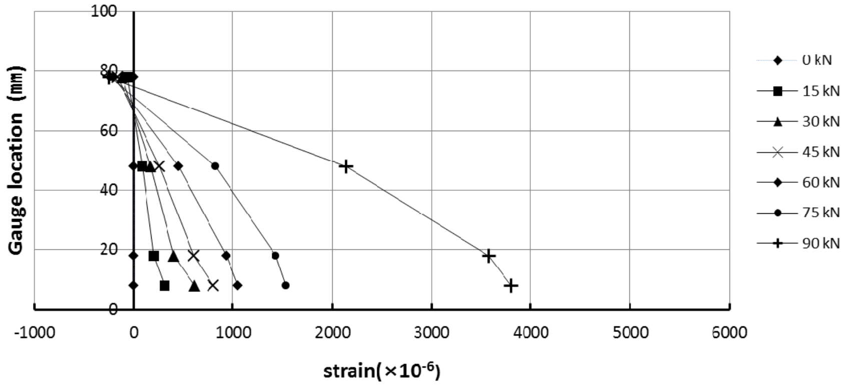

(a) B0 specimen

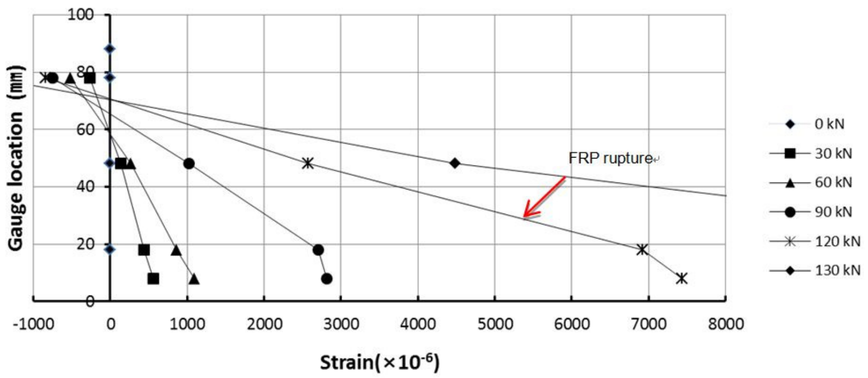

(b) B2 specimen

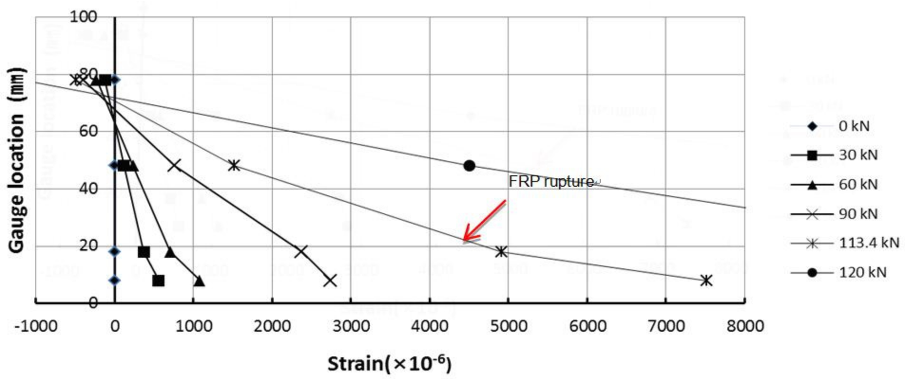

(c) B2-75% specimen

Fig. 8 Strain distribution mid-span cross section at load stage

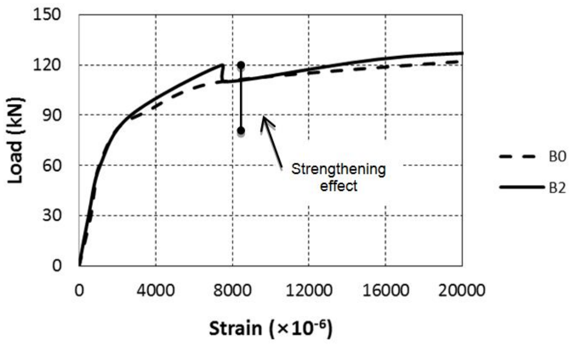

Fig. 9 Comparison of load-strain curve between B0 and B2 specimen

at 90 kN stage. After that, at 113.4 kN stage, large strain was observed at the bottom flange of the beam and CFRP was ruptured. The CFRP rupture load of the B2-75% specimen was lower than that of the B2 specimen.

2.2.5 Comparison for load-strain curve between B0 and B2

Fig. 9 shows the comparison for the load-strain curve for bottom flange of B0 and B2 specimens. For B0 specimen, the curve indicates that the strain was essentially linear until the yield load (82 kN) obtained from Eq. (1). The strain of bottom flange was about 0.20%. After that stage, the load was not clearly increased with increasing of strain known as the plastic range. For B2 specimen, the strain was linearly increased until the yield load (82 kN). However, after the yield load (82 kN), the load was apparently increased with increasing of strain until CFRP rupture load (113 kN), unlike B0 specimen. This means that CFRP sheet is showing a strengthening effect after yield load 82 kN. The measured CFRP sheet strain occurring at bottom flange of mid-span was about 0.95%. This is slightly less than the ultimate strain of the CFRP sheet subject to pure tension conditions, determined by the manufacture to be 1.20%.

3. Compression test

3.1 Test plan

3.1.1 Concept of retrofitting effect for CFRP strengthened columns

Fig. 10 shows the CFRP retrofitting concept on the compression member Square HSS (hollow steel section) in this study. Fig. 10 (a) shows a schematic of typical failure mode for a short HSS column. From the figure, it is observed that two sides would typically buckle outward and the other two sides would buckle inward. CFRP sheets can confine the outward buckling and transverse CFRP layers are effective at confining the outward local buckling of two opposite steel sides. This confinement controls the local buckling of HSS columns, and it can improve the axial capacity of HSS short columns. The long-column generates overall buckling as shown in Fig. 10(b), and in the cause of overall buckling occurrence (as shown in Fig. 10(b)), one section has tension on another section with different compressive force. Among them, when the FRP sheet is strengthened in the longitudinal direction on the HSS surface (as shown in Fig. 10(b)), tension reinforcement effect can be expected through the CFRP reinforcement on the HSS surface.

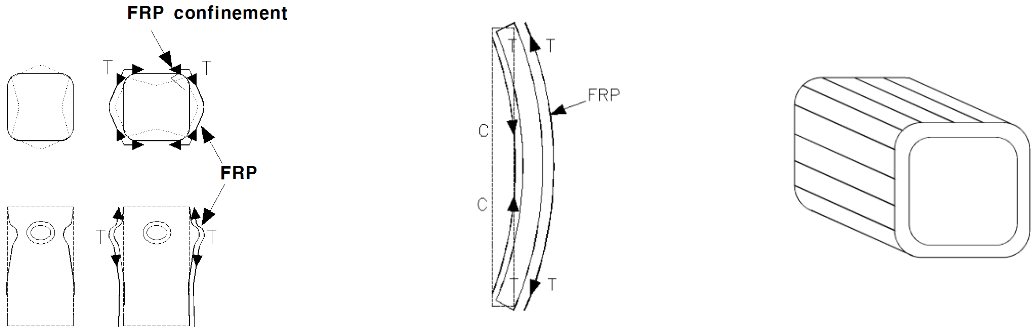

(a) Short column (b) Long column

Fig. 10 Schematic of typical failure mode for square HSS column

3.1.2 Test parameters and preparation

Six short-column and three long-column specimens were fabricated, and the test parameters were width-thickness ratio (b/t), length of columns, and number of CFRP layers. The AISC provision (AISC 2010) classifies the cross section by non-compact section and slender section according to the width-thickness ratio for column subjected to uniform compression. Firstly, in order to set the test parameter for width-thickness ratio, test parameters were selected for cross-sections that have width-thickness ratios lower or higher than the limit width-thickness ratio ($b/t = 1.40\sqrt{E/F_y}$) for non-compact sections, and slender section for short column subjected to uniform compression. The specimen is b/t = 20, 60. First, for the b/t = 20 specimen, 75 × 75 × 3.2 mm HSS (hollow square section) was produced. The length of the specimen is three times the cross-sectional width of 225 mm. For the b/t = 60 specimen, there was no pre-existing product; therefore, the 2.3 mm thick steel plate (2.2 mm as a measurement with vernier calipers) was bended in channel form and argon welding method was used to prevent deformation to produce a width of 138 mm for HSS section. The length of the specimen was three times the cross-sectional width of 414 mm. Also, for the load to be distributed evenly on the HSS, the end plate was welded to be produced. Secondly, for long columns, cross-sections had width-thickness ratios lower than the limit width-thickness ratio ($b/t = 1.40\sqrt{E/F_y}$) to satisfy the non-compact section condition. The long columns were fabricated using HSS section with 75 × 75 × 3.2 mm and the b/t was 20. Also, the length of specimens was made to be 21 times the width to observe the retrofitting effect of CFRP; for long columns the length of specimens were 1600 mm. The slenderness (kL/r) ratio was 38.5.

Finally, in this study, the number of CFRP layers was 0-ply, 1-ply, and 3-ply, respectively. When short HSS columns were subjected to compression load, two opposite sides would buckle outward and the other two sides would buckle inward. Therefore, transversely wrapping could control outward buckling (Fig. 11(a)). Also, when long HSS columns are subjected to compression load, where overall buckling takes place, FRP sheets oriented in longitudinal direction could provide tension reinforcement. Therefore, longitudinal wrapping was selected for long columns to control overall buckling, as shown in Fig. 11(b).

The list of specimens is summarized in Table 4. In the Table, there are three groups: SN, SS, and LN. Group SN means short non-compact section, and groups SS and LN mean short slender section and long non-compact section, respectively. The fiber direction for each group is shown in Figs. 11(a) and (b).

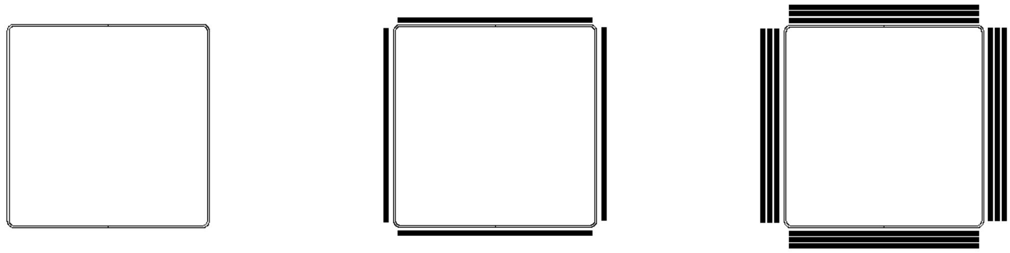

(i) Non-retrofitting (ii) 1-ply retrofitting (iii) 3-ply retrofitting

(a) Transversely retrofitting (Stub column)

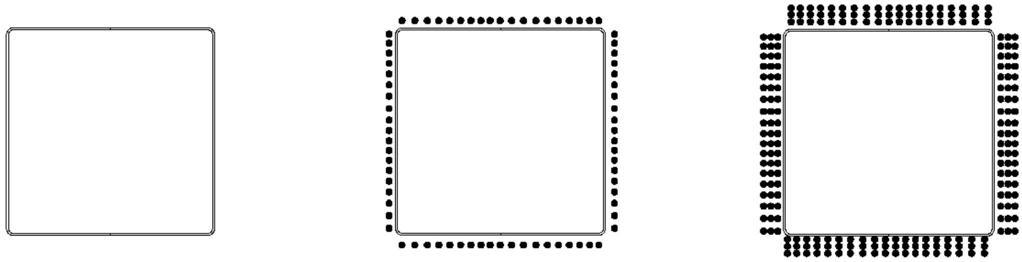

(i) Non-retrofitting (ii) 1-ply retrofitting (iii) 3-ply retrofitting

(b) Longitudinal retrofitting (Long column)

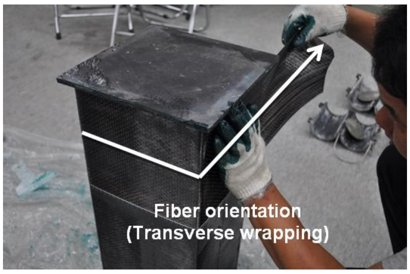

(i) Short columns

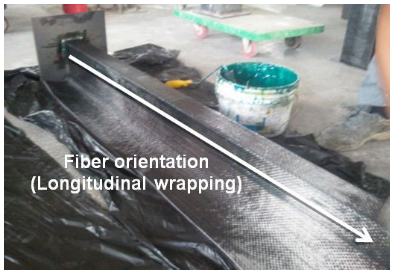

(ii) Long columns

(c) Overview of CFRP sheet retrofitting

Fig. 11 CFRP retrofitting on steel columns

3.1.3 Material test

Table 5 summarizes the material test results of steel plate. Material test results for 2.3 mm steel plates showed that the yield strength (F_y) was 288 MPa, tensile strength (F_u) was 371 MPa, and the elongation was 33%.

For 75×75×3.2 mm section, the actual thickness was 3.2 mm measured using vernier calipers. The yield strength (F_y) was 295 MPa and tensile strength (F_u) was 386 MPa, and the elongation was 23%.

The material test result on the CFRP is the same as the result mentioned in the flexural test part in Chapter 2, and the average thickness was 0.184 mm/ply, tensile strength was 2696 MPa, and modulus of elasticity was 224.6 GPa.

Table 4 Test parameter plan of compression test

Column type	Group	Specimen Label	Size (mm)	*b*/*t* (Nominal Value)	*b*/*t* (Actual Value)	Specimen length	Number of CFRP Ply	Fiber orientation
Short column	SN	SN-20-0	75×75×3.2	20	21.4	225	-	-
		SN-20-1T	75×75×3.2	20	21.4	225	1	T
		SN-20-3T	75×75×3.2	20	21.4	225	3	T
	SS	SS-60-0	142.6×142.6×2.3	60	62.7	414	-	-
		SS-60-1T	142.6×142.6×2.3	60	62.7	414	1	T
		SS-60-3T	142.6×142.6×2.3	60	62.7	414	3	T
Long column	LN	LN-20-0	75×75×3.2	20	21.4	1600	-	-
		LN-20-1L	75×75×3.2	20	21.4	1600	1	L
		LN-20-3L	75×75×3.2	20	21.4	1600	3	

*Note:
SN / SS / LN: Short- Non-compact / Short- Slender / Long- Non-compact
20 / 60 / 80 (*b*/*t* ratio): *b*/*t* = 20 / *b*/*t* = 60 / *b*/*t* = 80
0 / 1 / 3 (Number of CFRP ply): Non / 1ply / 3ply
T / L (Fiber orientation): (T) Transverse / (L) Longitudinal

Table 5 Material properties of steel plate

Steel thickness (mm)	Actual steel thickness (mm)	Elastic modulus (GPa)	Yield strength (MPa)	Ultimate strength (MPa)	Elongation percentage (%)
2.3	2.2	207	288	371	33
3.2	3.2	192	295	386	23

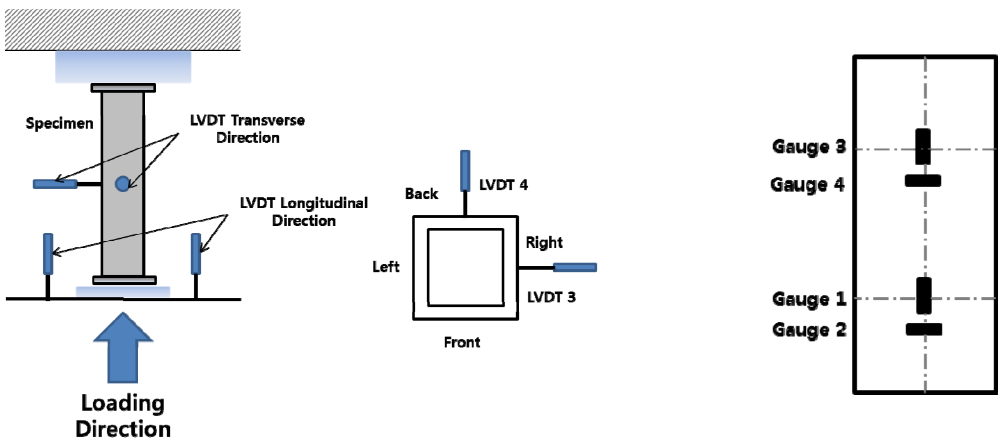

(a) LVDT Plan (SS, SN, group) (b) Strain gauge Plan (SS, SN, group)

Fig. 12 Measuring instrument plan and test set up

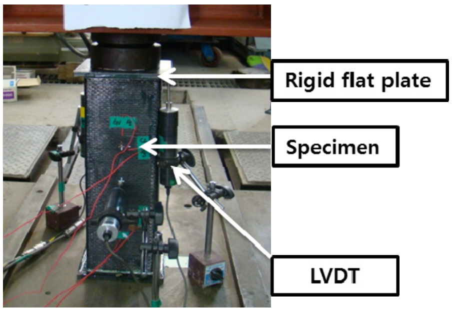

(c) Test setup (SS, SN group)

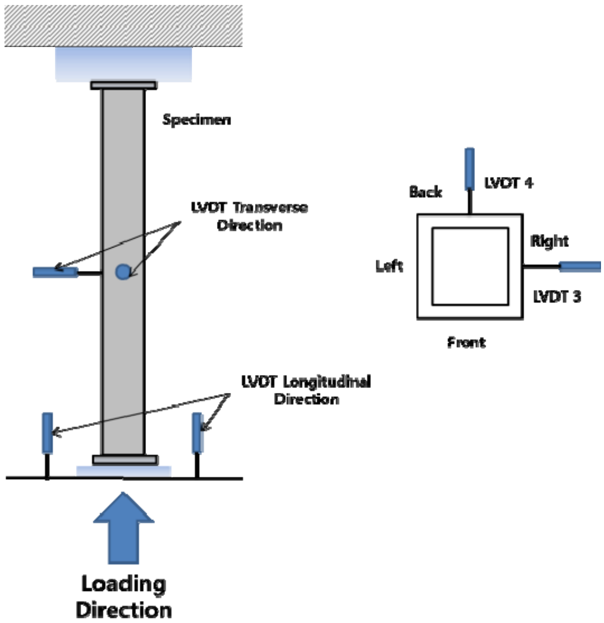

(d) LVDT Plan (LN group)

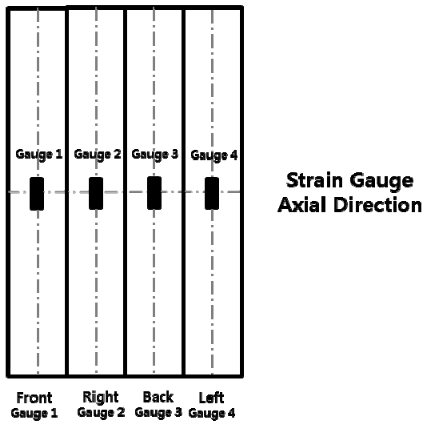

(e) Strain gauge Plan (LN group)

(f) Test setup (LN group)

Fig. 12 Measuring instrument plan and test set up

3.1.4 Test setup and instrumentation

Fig. 12 shows specimen setup and measuring instrument plan. Axial compression tests were conducted in a 2000 kN-class UTM (Universal Testing Machine). To measure displacement in the longitudinal direction, on each corner of the end plates two pieces of 50 mm LVDTs (Linear Variable Differential Transducers) were installed, and the average of the 2 values was determined to be the longitudinal displacement. Also, for LN groups, to measure lateral displacement, two pieces of 50 mm LVDTs (Linear Variable Differential Transducers) were installed at the center of the column. For SN and SS groups, the strain gauges were installed at a location between 1/3 spot and 2/3 spot for each of the specimens in the longitudinal direction and transverse direction as shown in Fig. 12(b). Strains in the longitudinal direction and the transverse direction were measured. Finally, for LN group, longitudinal direction strain gauges were installed at the center spot of the column to be expected to have maximum lateral deformation.

3.2 Test results and discussion

3.2.1 Specimen failure mode (SN and SS group)

Figs. 13(a)~(f) show the final failure mode detail for SN and SS groups, respectively. From the test, as shown in Figs. 13(a)~(f), on 2 of the 4 sides, an inward local buckling occurred and on the other 2 sides, an outward local buckling occurred when they were destroyed. For CFRP strengthened columns, as shown in Figs. 13(b), (d), and (f), on the 2 sides, inward local buckling occurred on the steel plate. In addition, on the other 2 sides, outward local buckling occurred, followed by the CFRP sheet rupturing as they were destroyed whenever the outward local buckling zone was expended. The failure modes of SS group was similar to those of SN group, having an inward local buckling on 2 of the 4 sides and an outward local buckling on the other 2 sides when they failed.

3.2.2 Specimen failure mode (LN group)

Fig. 13(g) shows the final failure mode detail for LN group. Unlike SN and SS groups, all specimens except LN-20-3L failed mainly due to overall buckling, as shown in Fig. 13(g). Then, secondary local buckling was followed at the maximum lateral displacement point. As shown in Fig. 13(g), the transverse displacement shows a decrease according to the increase in the number of CFRP layers (the measurement result on the transverse displacement is to be further discussed). Local buckling occurred in the form of an inward buckling of the compression flange and outward buckling of the two sides of web, as shown Figs. 13(h)~(j). For LN-20-1L specimen, secondary local buckling occurred at the compression surface region and CFRP sheet was ruptured at the tension surface region. However, for LN-20-3L specimen, only local buckling was observed at the bottom of the column, as shown in Fig. 13(g). This is because the strong CFRP tension reinforcement can effectively prevent the overall buckling. The final failure mode was similar to the short column's final failure shape, having two sides of inward local buckling and two sides of outward local buckling.

3.2.3 Load-displacement curves for column test

Figs. 14(a)~(c) shows the load-axial displacement of the SN group. In the initial loading stage, each specimen increased in load linearly and started to decrease in load increase rate after the elastic section. Among the SN group, as a result of comparing the load-displacement curve of the specimen (SN-20-1T, 3T) strengthened with control specimen (SN-20-0T) and CFRP, the maximum load showed to increase according to the number of CFRP.

(a) SN-20-0T (b) SN-20-1T (c) SN-20-3T

(d) SS-60-0T (e) SS-60-1T (f) SS-60-3T

(g) LN group specimens

(h) Local buckling at mid-part (LN-20-0L) (i) Local buckling at mid-part (LN-20-1L) (j) Local buckling at end part (LN-20-3L)

Fig. 13 Final specimen failure shape

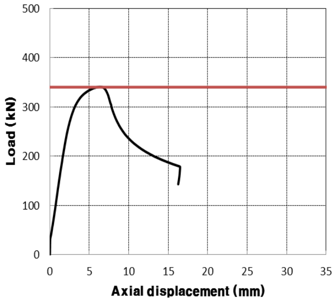

(a) SN-20-0T

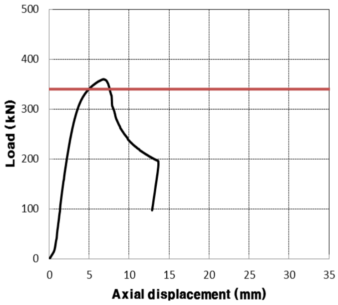

(b) SN-20-1T

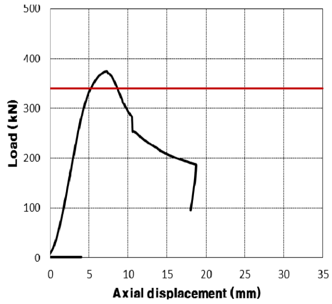

(c) SN-20-3T

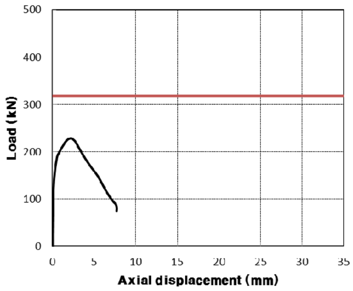

(d) SS-60-0T

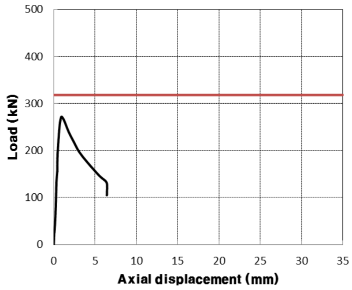

(e) SS-60-1T

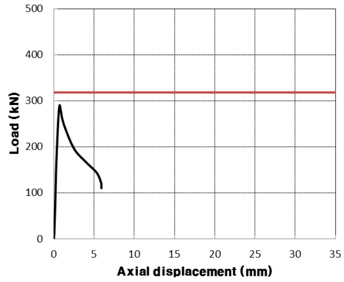

(f) SS-60-1T

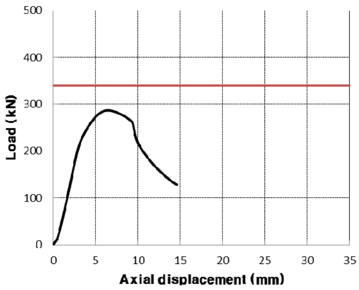

(g) LN-20-0L

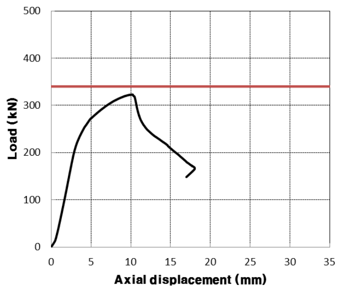

(h) LN-20-1L

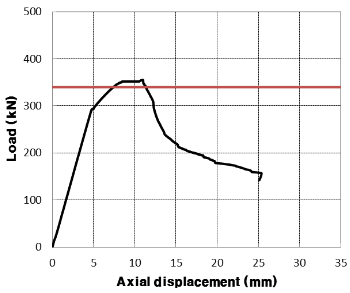

(i) LN-20-3L

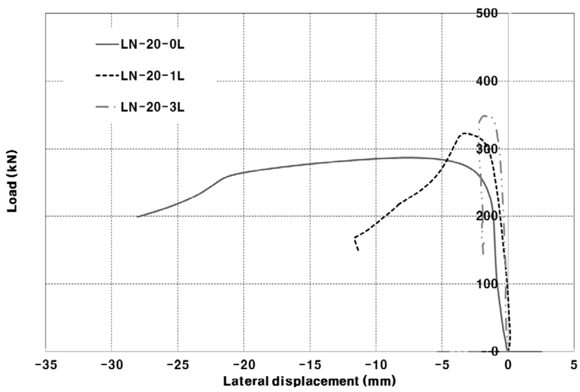

(j) Load-lateral displacement curve for LN group specimen

Fig. 14 Load-displacement curves for column specimens

Figs. 14(d)~(f) shows the load-axial displacement of the SS group. Like the SN group, in the initial yield section, the load increased linearly and showed the tendency to decrease in strength after the maximum load. However, in the other two specimens (not including SS-60-3T specimen), there was a decrease in the load before reaching yield load (P_y) due to the occurrence of local buckling; in other words, elastic buckling behavior is shown. The maximum load is shown to increase in strength as the number of reinforcement layers of the CFRP sheet increase. This is because the width to thickness ratio has a slender section above standards, and is affected by the elastic buckling behavior to result in specimen failure. Also, due to the reinforcement of the CFRP sheet, local buckling is delayed for the increase in the elastic buckling stress to be observed.

Figs. 14(g)~(i) shows the load-axial displacement of the LN group. Like the SN group, in the initial stage, the load increased linearly to show rapid reduction in the load after the maximum strength point. However, the maximum load was to be reduced more than the SN group. This is considered because of the characteristics of the long-column; the overall buckling is effected to reduce the strength. Accordingly, the LN-20-0L and LN-20-1L specimens did not reach the yield strength (P_y) value (the straight-line graph on the graph), and the specimen failed. Also, in comparison with the control specimen (SL-20-0L), the maximum strength value showed to increase as the number of reinforcement layers of the CFRP sheet increased.

Fig. 14(j) shows the load-lateral displacement of the LN-group. As shown in the figure, the lateral displace from overall buckling decreased due to the reinforcement of the CFRP sheet, and this effect is shown to increase clearly as the reinforcement amount increases. Especially, the LN-20-3L specimen was approximately 3 mm in lateral displacement to show that overall buckling did not occur, and the reinforcement of the CFRP sheet controlled the overall buckling shown in the long-column specimen to secure the stability on the buckling.

3.2.4 Load-strain curves for column test

Fig. 15 shows the load-strain curve on the compression member specimen. For the SS group and the SN group, between the 1/4-point and 3/4-point, where the strain gauge was measured, the measurement value of the point in which the local buckling occurred is summarized in Fig. 15. In the case of LN Group, the strain gauge is installed in the mid-span section; therefore, the result value measured from the mid-span section was summarized. In Fig. 13, the straight line shows the yield load ($P_y = A_s \times F_y$), and the dots indicated on the graph are the occurrence points of the local buckling. Figd. 15(a)-(c) shows the load-strain curve of the SN group. As the load increased, the strain was shown to decrease rapidly due to the occurrence of local buckling. Like the behavior characteristic of the non-compact section, the strain was shown to increase rapidly near the yield strength due to the occurrence of local buckling, and with the reinforcement of the CFRP sheet, the local buckling occurrence point was delayed and the specimen with local buckling occurring after the yield load was observed (Figs. 15(b) and (c)).

Figs. 15(d)~(f) shows the load-strain curve of the SS group. In the case of the SS group, like the characteristics of the slender section, local buckling was occurred before the yield load to show the decreasing behavior in the load, as shown in the result measured on the strain gauge on Figd. 15(d)~(f); rapid deformation was shown to be occurring before the yield load. In the SS-60-3T specimen, increased load of local buckling occurrence was observed as shown in Fig. 15(f), and due to the reinforcement of the CFRP sheet, the local buckling occurrence point was delayed to have the performance observed up to the yield load.

Figs. 15(g) and (i) shows the load-strain curve of the LN group. LN group showed that as the load increases, due to the characteristics of the long-column specimen, the overall buckling before

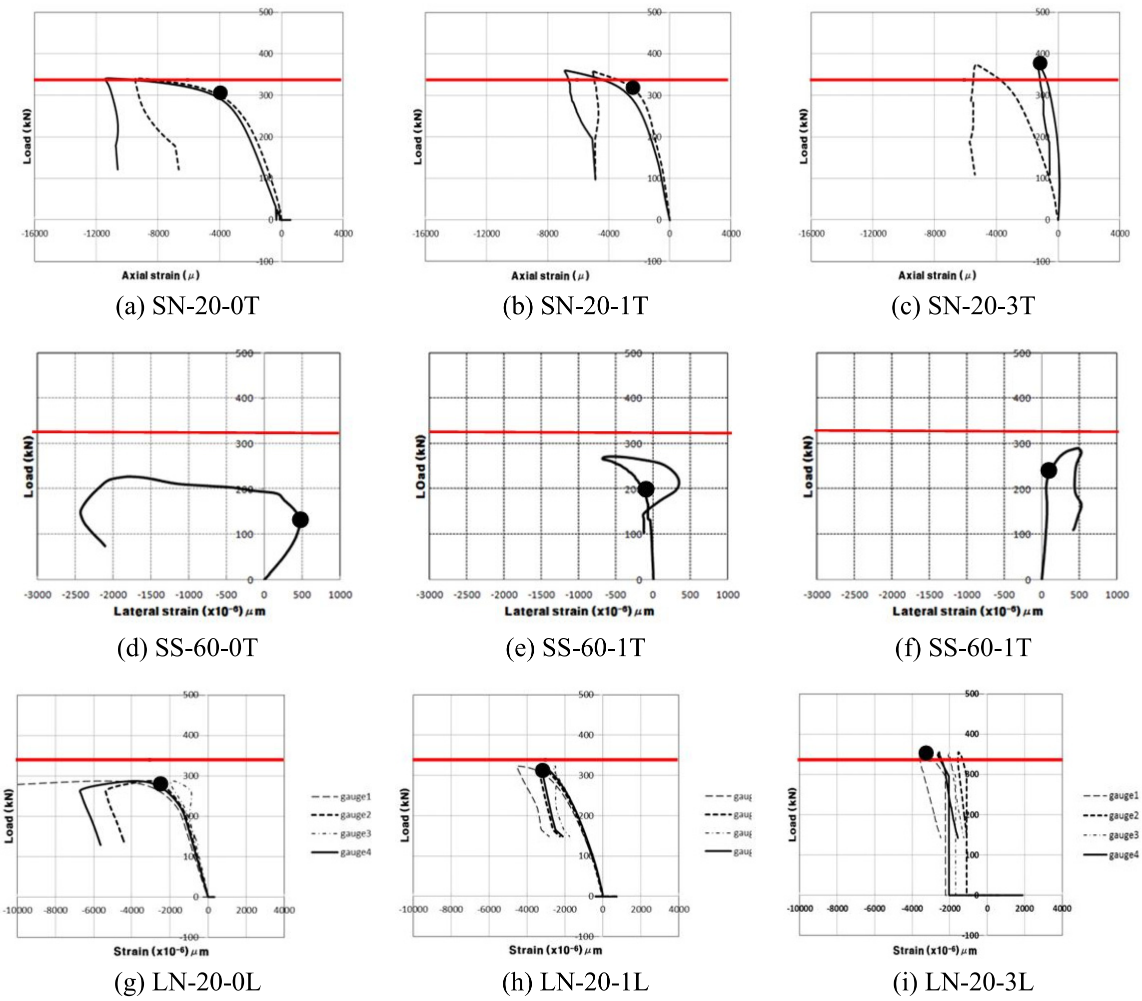

(a) SN-20-0T (b) SN-20-1T (c) SN-20-3T

(d) SS-60-0T (e) SS-60-1T (f) SS-60-1T

(g) LN-20-0L (h) LN-20-1L (i) LN-20-3L

Fig. 15 Load-strain curve for column specimens

the yield strength was affected to clearly increase in strain. Among them, in Figs. 15(g) and (h) graph, the compression strain was observed to occur and change in strain direction afterwards (Figs. 15(g): gauge 3 and 14(h): gauge 3). This specified that the section bonded to gauge No. 3 received tensile strain after the progression of compressive deformation and the occurrence of flexural buckling. Through this, we can see that the LN groups will be dominated by the overall buckling failure mode.

3.2.5 Load and stiffness effect on number of CFRP layer

Table 6 summarizes the test result values for the yield load (P_y), maximum load, and the initial stiffness for each specimen. Fig. 15 shows the ratio of increasing rate for the maximum load according to the CFRP sheet ply of each specimen for the SS, SN, and LN group. As a result of the test, as the number of CFRP layers increased, the maximum load was shown to increase. The load was increased a maximum of 10.0% in the SN group, 57.0% in the SS group, and 18.0% in the LN group, respectively, to verify the strengthening effect of the CFRP sheet. Generally, considering that the HSS is insufficient in strength improvement effect due to the additional external confinement, the strengthening effect of the SN group is shown to not be very large. However, in the case of SS group (composed of slender section), the specimens were reduced in strength before reaching the yield strength due to the local buckling, and from the constraint effect of the CFRP sheet, the local buckling was delayed and the stress of the elastic buckling was increased for the increase in load to be observed. Therefore, the strengthening effect from the confinement of the CFRP sheet in the HSS was more effective on the slender section rather than the non-compact section. Also, the long-column of LN group receives tension on one section of the HSS from the flexural buckling, and the increase in load was observed from the flexural strengthening effect according to the longitudinal-direction reinforcement of the CFRP sheet. The strength increase rate of each specimen was summarized in the Fig. 14.

Stiffness was calculated by the concept in Fig. 5, and the result value was summarized in the Table. As a result of the analysis, a maximum of 7% increase was shown centrally of the control specimen to show that the reinforcement of CFRP sheets did not affect stiffness.

3.2.6 Ductility effect on number of CFRP layer

Ductility is defined using the ratio of failure displacement (δ_u) and yield displacement (δ_y) obtained from in Eq. (3). The failure displacement (δ_u) is defined as the 85% of maximum load (Park and Choi 1998). The yield displacement and failure displacement are calculated through the load-axial displacement curve and the calculated DI (ductility index) values are summarized in Table 6.

$$DI = \frac{\delta_u}{\delta_y} \tag{3}$$

Where, DI is ductility index and δ_u and δ_y are the displacement at maximum load and yield load (refer Eq. (2)), respectively.

The results of effects of DI (Ductility index) depending on the number of CFRP layers are summarized in Table 6. For non-compact section (SN, LN group), DI was seen to be generally

Table 6 Test results for column test

Column type	Group	Specimen label	Specimen length	b/t	P_{max} (kN)	% in gain or loss	Stiffness (kN/mm)	% in gain or loss	DI	% in gain or loss
Short column	SN	SN-20-0	225	20	340.8	Control	66.6	Control	2.67	-
		SN-20-1T	225	20	359.9	6.0	65.4	-2.0	2.70	1.1
		SN-20-3T	225	20	374.7	10.0	68.0	2.0	3.33	24.7
	SS	SS-60-0	414	60	228.0	Control	328.7	Control	6.7	-
		SS-60-1T	414	60	271.0	19.0	304.7	-7.0	3.20	-54.2
		SS-60-3T	414	60	358.3	57.0	310.6	-6.0	3.07	-55.4
Long column	LN	SN-20-0	1600	20	286.9	Control	59.4	Control	3.16	-
		LN-20-1L	1600	20	322.9	13.0	56.3	-6.0	3.43	8.5
		LN-20-3L	1600	20	339.5	18.0	60.0	1.0	3.71	17.4

increasing as the number of CFRP ply increased. The 24.7% increasing of DI was shown for SN group specimens. This is due to CFRP sheet confining can delay the local buckling of HSS. Also, the 17.4% increasing of DI was shown for LN group specimens. This is due to CFRP sheet strengthening can provide the flexural performance and delay the overall buckling of long HSS column. As can be seen in Table 6, for SS group with b/t = 60, the DI was also decreased up to -55.4% as shown in Table 6. This can be thought as, in the case of SS-60-0T specimens (b/t = 60), the ductile behavior was maintained after the maximum load point. However, in the case of other 2 specimens (SS-60-1T, SS-60-3T), they could not produce ductile behavior due to the brittle properties of CFRP, after all, the DI decreased.

4. Conclusions

In this study, reinforcing with CFRP sheet on the steel-frame structure flexural member and the compression member, the flexural test and compression test of verifying the reinforcement effect were performed, and from the results, the following conclusions were derived. For the flexural test, the test parameters were the number of CFRP layers and the reinforcement length, and for the compression member, the test parameters were the number of reinforcement layers, width-thickness ratio, and the short & long-columns:

(1) For the flexural test, the un strengthened specimen of B0 was executed with flexural failure showing sufficient plastic behavior, and in the case of the strengthened specimen, the mid-span section of the CFRP sheet failed; as the load increases, the delamination failure behavior of the steel surface and the CFRP sheet separating was shown.

(2) The initial stiffness showed a maximum of 6.71% increase rate in contrast to the control specimen (B0) according to the number of CFRP layers and the reinforcement length, showing that the number of CFRP layers and the reinforcement length do not affect the initial stiffness.

(3) As the number of reinforcement layers increased, the yield strength increased 31.7%, and failure strength of CFRP failure was shown to increase maximum of 11.30%. Therefore, it was concluded that as the number of reinforcement layers of the CFRP sheet increased, the strength also increased.
Examining the strengthening effect according to the reinforcement length, for the B2-50% specimen in comparison to the B2 specimen, the yield load decreased a maximum of -11.8% and the failure load decreased a maximum of -10.4% to show that the load reduction rate increases as the reinforcement length decreased. Also, the load was reduced from the decrease in the reinforcement length, and based on the test result to secure the original strength; the reinforcement length must be approximately 92% of the span.

(4) In the flexural specimen, the initial stiffness showed a maximum of 6.71% increase rate compared to the control specimen (B0) according to the number of CFRP layers and reinforcement length, to verify that the number of CFRP layers and the reinforcement length did not affect the initial stiffness.

(5) In the compression test, for the short-column, the two sections occurred with inward local buckling and the other two sections occurred with outward local buckling to result in failure. The CFRP sheet ruptured due to the outward local buckling to result in failure. Also, due to the member length effect, the long-columns occurred with overall buckling,

and the three-layer strengthened specimen, LN-20-3L controlled the overall buckling through sufficient reinforcement ratio of the CFRP sheet and it had the local buckling on the member end part.

(6) For the strengthening effect of the CFRP sheet, in the short-column specimen, the non-compact section of the SN group increased a maximum of 10% in load according to the increase in the number of CFRP layers, and in the slender-section of SS group, the strength increased up to 57% to verify that the strengthening effect increased even more in the HSS composed of slender elements. For the long-column specimen of LN group, the strength increased a maximum of 18% according to the increase in the number of CFRP layers.

(7) In the compression specimen, the initial stiffness was ranged from 2.0% to 7.0% for each group according to the number of CFRP layers. Therefore, it was shown that the number of CFRP layers did not effect on the initial stiffness. However, the ductility index (DI) was improved for SN, LN group specimens according to the number of CFRP layers. However, for SS group, the (DI) was decreased with increasing the number of CFRP layers. For shore column specimens, two sections occurred with inward local buckling, and the other two sections occurred with outward local buckling. Through the lateral transverse confinement of the CFRP sheet to constrain the deformation from local buckling, reinforcement effect was shown. Also, the long-column had flexure due to the overall buckling; the flexure could control by the longitudinal direction reinforcement of the CFRP sheet.

References

AISC (2010), Steel Construction Manual; Volume 2, (13th Ed.), American Institute of Steel Construction.

Fam, A., Macfougall, C. and Shaat, A. (2009), "Upgrading steel-concrete composite girders and repair of damaged steel Beams using bonded CFRP laminates", *Thin-Wall. Struct.*, **47**(1), 1122-1135.

Harries, K.A., Peck, A.J. and Abraham, E.J. (2009), "Enhancing stability of structural steel sections using FRP", *Thin-Wall. Struct.*, **47**(1), 1092-1101.

Miller, T.C., Chajes, M.J., Mertz, D.R. and Hastings, J.N. (2001), "Strengthening of a steel bridge girder using CFRP plates", *ASCE*, *J. Bridge. Eng.*, **6**(6), 514-522.

Park, J.W. and Choi, S.M. (2013), "Structural behavior of CFRP strengthened concrete-filled steel tubes columns under axil compression loads", *Steel Compos. Struct.*, *Int. J.*, **14**(5), 453-472.

Photiou, N.K., Hollaway, L.C. and Chrassanthopoulos, M.K. (2006), "Strengthening of an artificially damaged steel beam utilizing a carbon/glass composite system", *J. Construct. Mater* ., **20**(1), 11-21.

Ritchie, P.A., Toamas, D.A., Lu, W. and Conneilly, G.M. (1991), "External reinforcement of concrete beams using fiber reinforced plastics", *ACI Structural J.*, 490-500.

Sallam, H.E.M., Badawy, A.A.M., Saba, A.M. and Mikhail, F.A. (2010), "Flexural behavior of strengthened steel-concrete composite beams by various plating methods", *J. Const. Steel. Res.*, **62**(1), 472-483.

Schnerch, D. and Rizkalla, S. (2008), "Flexural strengthening of steel bridges with high modulus CFRP strips", *ASCE J. Bridge Eng.*, **13**(2), 192-201.

Shaat, A. and Fam, A.Z. (2006), "Axial loading tests on short and long hollow structural steel columns retrofitted using carbon fibre reinforced polymers", *Can. J. Civil Eng.*, **33**(4), 458-470.

Shatt, A. and Fam, A. (2008), "Repair of cracked steel girders connected to concrete slabs using carbon fiber reinforced polymer sheets", *J. Compos. Construct..*, **12**(6), 650-659.

Shaat, A. and Fam, A.Z. (2009), "Slender steel columns strengthened using high-modulus CFRP plates for buckling control", *ASCE*, *J. Compo. Const.*, **13**(1), 1-12.

Swamy, E.N., Johns, E. and Charif, A. (1989), “The effect of external plate reinforcement on the strengthening of structurally damaged RC beams”, *The Structural Engineer*, **67**(3), 45-54.
Zhao, X.L. and Zhang, L. (2007), “State of art review on FRP strengthened steel structures”, *Eng. Struct.*, **29**(8), 1808-1823.

CC